Quantum Monte Carlo study of the spin-1/2 honeycomb Heisenberg model with mixed antiferromagnetic and ferromagnetic interactions in external magnetic fields

Yi-Zhen Huang
CAS Key Laboratory of Vacuum Physics, School of Physical Sciences, University of Chinese Academy of Sciences, P. O. Box 4588, Beijing 100049, China

Gang Su*
Kavli Institute for Theoretical Sciences, and CAS Key Laboratory of Vacuum Physics, School of Physical Sciences, University of Chinese Academy of Sciences, Beijing 100049, China

(Received 14 December 2016; revised manuscript received 19 April 2017; published 30 May 2017)

The continuous imaginary-time quantum Monte Carlo method with the worm update algorithm is applied to explore the ground-state properties of the spin-1/2 Heisenberg model with antiferromagnetic (AF) coupling $J > 0$ and ferromagnetic (F) coupling $J' < 0$ along zigzag and armchair directions, respectively, on honeycomb lattice. It is found that by enhancing the F coupling J' between zigzag AF chains, the system is smoothly crossover from one-dimensional zigzag spin chains to a two-dimensional magnetic ordered state. In absence of an external field, the system is in a stripe-ordered phase. In the presence of uniform and staggered fields, the uniform and staggered out-of-plane magnetizations appear while the stripe order remains in the xy plane, and a second-order quantum phase transition (QPT) at a critical staggered field is observed. The critical exponents of correlation length for QPTs induced by a staggered field for the cases with $J > 0$, $J' < 0$ and $J < 0$, $J' > 0$ are obtained to be $\nu = 0.70046(1)$ and $0.7086(3)$, respectively, indicating that both cases belong to O(3) universality. The corresponding dynamic and susceptibility exponent z and γ/ν are fitted to be 1.006572(9), 1.9412(2) and 1.004615(8), 1.96121(9) for the two cases, respectively. The scaling behavior in a staggered field is analyzed, and the ground-state phase diagrams in the plane of coupling ratio and staggered field are presented for two cases. The temperature dependence of susceptibility and specific heat of both systems in external magnetic fields is also discussed. A Kosterlitz-Thouless phase transition is found for the present system in a uniform field.

DOI: 10.1103/PhysRevE.95.052147

I. INTRODUCTION

Since the spin-1/2 antiferromagnetic (AF) Heisenberg model is believed to be capable of describing the undoped precursors of high-temperature superconducting cuprates, it has attracted intensive attention in condensed matter and statistical physics. Through extensive explorations both theoretically and experimentally in the past few decades, many properties of this model have been exposed, and a great deal of advances have been achieved. However, as the complexity occurs intrinsically in many-body systems, there are still a lot of ambiguities remaining to be investigated. For instance, by searching for exotic states of matter or studying quantum phase transitions (QPTs), people usually invoke this model with different interactions on various lattices as prototypes. To name but a few, quantum spin liquid is thought to exist in spin-1/2 AF Heisenberg models on lattices with geometrical frustrations, but its nature is still under active debate [1–8]; whether exotic phase transitions beyond the traditional Landau-Ginzburg-Wilson framework [9] exist was also discussed by introducing more complex interactions or by tuning the spatial anisotropy in coupling strength, and so on.

It has been shown that the spin-1/2 AF Heisenberg system on square lattice displays Néel order in ground state with the staggered magnetic moment per site $m_s \cong 0.3075$ by quantum Monte Carlo (QMC) [10] and $m_s \cong 0.3034$ by the spin-wave theory [11], while the one-dimensional (1D) spin 1/2 AF spin chain is magnetically disordered with gapless excitations. The experimental results that the quasi-1D spin-1/2 AF chains Sr_2CuO_3 and Ca_2CuO_3 [12] exhibit low Néel temperatures and extremely small ordered moments trigger an interesting question: How does the AF long-range order in two-dimensional (2D) lattice (like square lattice) in ground states develop from coupled 1D spin chains with increasing interchain interactions? Several studies tackle this issue and the critical interchain coupling ratio $R_c = J_\perp/J$ was determined as follows: The spin-wave theory gives $R_c = 0.034$ [13], one-loop renormalization group analysis on an effectively spatially anisotropic nonlinear σ model yields $R_c = 0.047$ [14], the series expansion numerical techniques bound R_c from upper to 0.02 [15]; whereas some self-consistent calculations [16] and exact diagonalization [17] predict it as high as 0.15 and 0.1–0.2, respectively. According to the exact result of Bethe ansatz or the results of, e.g., spin-wave theory with random-phase approximation [18] and mean-field approaches [19], the spin-1/2 AF Heisenberg chain is critical and it is confirmed by using the multichain mean-field method associated with a Monte Carlo algorithm [20,21] on AF square lattices. Here we intend to study this issue on a honeycomb lattice with ferromagnetic (FM) armchair bonds (interchain) and AF zigzag chains by tuning the coupling ratio, as the honeycomb lattice has a smaller coordinate number and stronger quantum fluctuations than square lattice. We also wish to further understand the ground-state and thermodynamic properties as well as the scaling behaviors and topological phase transitions of the system under interest in uniform and staggered magnetic fields.

*Corresponding author: gsu@ucas.ac.cn

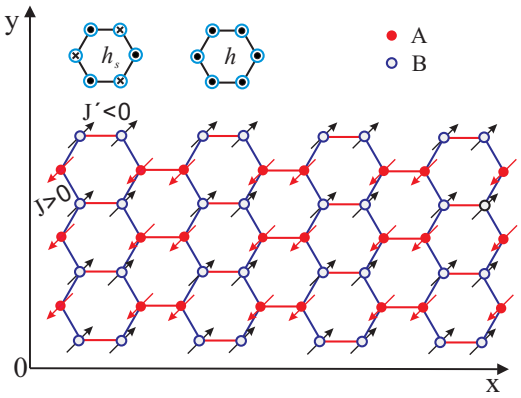

FIG. 1. The spin-1/2 Heisenberg model on honeycomb lattice with antiferromagnetic (AF) and ferromagnetic (F) interactions between nearest-neighbor spins (indicated by arrows) along zigzag (blue bonds along the y direction) and armchair (red bonds along the x direction) chains, respectively. The red solid dots and blue open circles indicate the lattice sites on sublattices A and B, respectively, and in the two hexagons in the inset the directions of the uniform (h) and staggered (h_s) magnetic fields are shown.

Alternatively, one can study 2D anisotropic Heisenberg AF models with different bond interactions to observe crossover behaviors by tuning the bond interactions. For instance, such attempts were made on honeycomb lattice with the dimer pairs pinned on the armchair bonds by using the methods of tensor renormalization group [22] and QMC [23], where it is found that there is a QPT of classical O(3) universality from a disordered dimer phase to quantum Néel order at a critical interdimer AF interaction. In our previous work [24], we replaced the interdimer AF couplings by ferromagnetic (F) interactions along zigzag directions on honeycomb lattice and found that there is also a phase transition from a dimerized phase to a stripe phase. The scaling behaviors were analyzed, and the coupling parameters of two compounds were estimated by comparing our QMC calculated results.

In contrast to this previous work [24], where the interactions are supposed to be F along the zigzag direction and AF along the armchair direction, for the completeness of the study, in this paper we shall consider the spin-1/2 Heisenberg model with mixing AF interaction (J) along the zigzag direction and the F interaction (J') along the armchair direction on a honeycomb lattice (Fig. 1) in magnetic fields. It should be noted here that the present system (we refer to Case A later) differs considerably from that considered in Ref. [24] (we refer to Case B later), and the two systems cannot be transformed mutually by simply using a unitary transformation. This observation is confirmed by our QMC studies, where we observe that a small interchain F interaction could make the 1D disordered state smoothly crossover to a 2D spin-ordered state. In the presence of uniform and staggered fields, the uniform and staggered magnetizations in the z direction appear while a stripe order remains in the xy plane, and a second-order QPT at a critical staggered field is observed. Although there is a zero magnetization plateau in the honeycomb spin ladder with AF legs and F rungs in $m_z \sim h$ curves [25], no zero magnetization plateau exists for both cases with $J' = -J$ due to the appearance of spin order. The phase diagram in a staggered field is also presented.

This paper is organized as follows. In Sec. II, we shall give the model Hamiltonian, calculational method, and definitions of several physical quantities. The crossover behavior from 1D to 2D in the absence of a magnetic field is discussed in Sec. III; the magnetization in the presence of uniform and staggered external magnetic fields is presented in Sec. IV; and the finite-size scaling analysis is given in Sec. V. Section VI shows the phase diagrams of two systems for a comparison; the temperature dependence of specific heat and susceptibility in magnetic fields is discussed in Sec. VII; in Sec. VIII a Kosterlitz-Thouless (KT) transition is presented for finite temperature conditions; and, finally, a summary is given.

II. MODEL, METHOD, AND DEFINITIONS

A. Model

By using the continuous imaginary-time QMC with worm update algorithm, we shall study the spin-1/2 Heisenberg model on a honeycomb lattice with mixing AF and F interactions along the zigzag and armchair directions, respectively, as depicted in Fig. 1, in the presence of uniform or staggered magnetic fields. The AF interactions separate the lattice into sublattices A and B, correspondingly denoted by red solid dots and blue blank circles in Fig. 1. The Hamiltonian of the system is

$$H = J\sum_{\langle ij\rangle_{ZZ}} \mathbf{S}_i\cdot\mathbf{S}_j + J'\sum_{\langle ij\rangle_{AM}} \mathbf{S}_i\cdot\mathbf{S}_j - h\sum_{i=1}^{N}\mathbf{S}_i^z - h_s\sum_{i=1}^{N}(-1)^i\mathbf{S}_i^z, \tag{1}$$

where $\mathbf{S}_i$ is the spin-1/2 operator at ith site; $\langle ij\rangle_{ZZ}$ and $\langle ij\rangle_{AM}$ denote nearest neighbors along the zigzag and armchair directions, respectively; $J > 0$ and $J' < 0$ are corresponding coupling constants; and h and h_s are the external uniform and staggered magnetic fields, respectively. We define the coupling ratio $\alpha_1 = \frac{J'}{J}$ for later use. For convenience, we also mark the armchair and zigzag directions by the x and y directions, respectively. $N = L_xL_y$ is the total number of lattice sites, where $L_{x(y)}$ is the length of x (y) direction.

From Sec. IV onward, we shall also make comparisons between the present system and the system with $J < 0$ and $J' > 0$ in the previous work [24] in a staggered field, where the coupling ratio is defined as $\alpha_2 = \frac{J}{J'}$.

B. Method

We shall use the continuous-time QMC with worm update algorithm to study the system under consideration. This algorithm expands the partition function of system as a summation of path integrals with continuous loops under Fork states representation with $\{|S_i^z\rangle\}$ as the basis in interaction picture by

$$\begin{aligned} Z &= \mathrm{Tr}(e^{-\beta H}) \\ &= \mathrm{Tr}(e^{-\int_0^\beta d\tau H}) \\ &= \sum_{n=0}^{\infty}(-1)^n\mathrm{Tr}\Big\{e^{-\beta H_0}\int_0^\beta d\tau_n \\ &\quad \ldots\int_0^{\tau_2} d\tau_1[H_{In}H_{I(n-1)}\ldots H_{I1}]\Big\}, \end{aligned} \tag{2}$$

where $\beta = \frac{1}{k_B T}$, the inverse temperature, acting as the length of the imaginary time in the simulation; $k_B = 1$ is the Boltzman constant; H_0 stands for the interaction between spins along the z direction

$$H_0 = J \sum_{\langle ij\rangle_{ZZ}} S_i^z S_j^z + J' \sum_{\langle ij\rangle_{AM}} S_i^z S_j^z - h \sum_{l=1}^{N} S_l^z - h_s \sum_{l=1}^{N} (-1)^l S_l^z; \tag{3}$$

and H_I is the hopping term in the xy plane of spin space

$$H_I = \frac{J}{2} \sum_{\langle ij\rangle_{ZZ}} (S_i^+ S_j^- + S_i^- S_j^+) + \frac{J'}{2} \sum_{\langle ij\rangle_{AM}} (S_i^+ S_j^- + S_i^- S_j^+). \tag{4}$$

In this framework, the object sampled during executing the algorithm is each term in Eq. (2), and the integration is concretized to several configurations with special localizations of off-diagonal terms in the imaginary time axis. In lattice space and imaginary time coordination, such configurations are graphed as multiple worldlines with only continuous loops. By introducing the kink pair $S_{i\tau_1}^+ S_{i\tau_2}^-$, called a worm, a partition function configuration is switched into a Green function configuration. The hopping of the worm ends ($S_{i\tau}^+$ or $S_{i\tau}^-$) along the imaginary time or the real space direction realizes the sampling of the Green functions and the ends' annihilation finishes an update from an old Z configuration to a new one [26,27]. The big difference between the partition function configuration and the Green function configuration is that the latter has an extra discontinuous worldline, i.e., the worm. This method extends the sampling space and could be used to calculate the winding number directly.

C. Definitions

Before we proceed further, we first give the definitions of relevant physical quantities that will be used later. As the calculations based on the QMC method are usually associated with the finite-size systems, where the spin $O(3)$ rotational symmetry remains in a finite system, we should determine the order parameters by calculating the corresponding square values combined with a size extrapolation. The staggered magnetization per site is defined via the following expression:

$$\begin{aligned}\langle m_s^2\rangle &= \left\langle \left\{ \frac{1}{N} \left[\sum_{i\in A} (\mathbf{S}_i^x + \mathbf{S}_i^y + \mathbf{S}_i^z) - \sum_{j\in B} (\mathbf{S}_j^x + \mathbf{S}_j^y + \mathbf{S}_j^z) \right] \right\}^2 \right\rangle \\ &= 3\left\langle \left\{ \frac{1}{N} \left[\sum_{i\in A} \mathbf{S}_i^z - \sum_{j\in B} \mathbf{S}_j^z \right] \right\}^2 \right\rangle \\ &= \frac{3}{2}\frac{1}{N} \sum_{r=0}^{N-1} f(r) \langle S_0^+ S_r^- \rangle, \end{aligned} \tag{5}$$

where $f(r) = 1$ if both S_0^+ and S_r^- are in the same sublattice; otherwise, $f(r) = -1$, and r is the distance between lattice sites i and j.

The staggered magnetization per site in the xy plane in the presence of a uniform or staggered field can be studied through

$$\begin{aligned}\langle m_\perp^2\rangle &= \left\langle \left\{ \frac{1}{N} \left[\sum_{i\in A} (\mathbf{S}_i^x + \mathbf{S}_i^y) - \sum_{j\in B} (\mathbf{S}_j^x + \mathbf{S}_j^y) \right] \right\}^2 \right\rangle \\ &= \frac{1}{N} \sum_{r=0}^{N-1} f(r) \langle S_0^+ S_r^- \rangle. \end{aligned} \tag{6}$$

The uniform magnetization per site is defined by

$$m_z = \left\langle \frac{1}{N\beta} \sum_{i=1}^{N} \int_0^\beta S_{i\tau}^z d\tau \right\rangle. \tag{7}$$

The uniform magnetic susceptibility is given by

$$\chi_u = \frac{1}{N\beta} \left\{ \sum_{ij} \left\langle \int_0^\beta d\tau_1 d\tau_2 S_{i\tau_1}^z S_{j\tau_2}^z \right\rangle - \left\langle \int_0^\beta d\tau_1 S_{i\tau_1}^z \right\rangle \left\langle \int_0^\beta d\tau_2 S_{j\tau_2}^z \right\rangle \right\}. \tag{8}$$

The staggered magnetization per site in the z direction will be calculated by

$$m_z^s = \left\langle \frac{1}{N\beta} \sum_{i=1,j=1}^{L_x,L_y} (-1)^{i+j} \int_0^\beta S_{ij(\tau)}^z d\tau \right\rangle. \tag{9}$$

Here i and j denote the lattice site's index along the x and y directions. The spin stiffness ρ is obtained by the fluctuation of winding numbers [28]

$$\begin{aligned}\rho_\theta &= \frac{\partial^2 \Omega}{\partial^2 \Phi} = \frac{1}{\beta} \langle W_\theta^2 \rangle \\ &= \frac{1}{\beta} \langle [(N_\theta^+ - N_\theta^-)/L_\theta]^2 \rangle, \end{aligned} \tag{10}$$

where Ω is the free energy and Φ, W_θ, N_θ^+, N_θ^-, and L_θ are twisted angle at the boundaries, the winding number, the number of lattice sites for spin $\uparrow$ along the positive and negative θ directions, and the lattice width for the corresponding direction, respectively. It is noted that the spin stiffness ρ in Eq. (10) has its counterpart in a boson system [29,30], the superfluid density, which characterizes an off-diagonal long-range order.

We shall calculate the correlation lengths ξ_{zigzag} and ξ_τ along the zigzag direction (y direction) and the imaginary time β direction, respectively, through the canonical correlation function $C(\vec{q}, i\omega)$ [31,32] defined by

$$C(\vec{q}, i\omega) = \frac{1}{L_x L_y \beta} \left\langle \sum_{j,k=1}^{N} \int_0^\beta d\tau_1 \int_0^\beta d\tau_2 S_j^+(\tau_1) S_k^-(\tau_2) \times \exp\{-i[\omega(\tau_2 - \tau_1) + \vec{q} \cdot (\vec{r_k} - \vec{r_j})]\} \right\rangle, \tag{11}$$

where $i\omega = 2\pi/\beta$ is the lowest Matsubara frequency. The honeycomb lattice could be mapped to the brick-wall lattice.

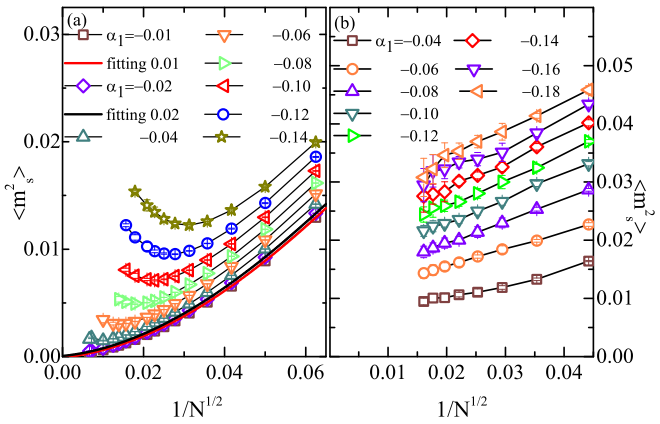

FIG. 2. The size extrapolation of the order parameter $\langle m_s^2 \rangle$ vs $\frac{1}{\sqrt{N}}$ for (a) $L_x = L_y = L$ and (b) $L_y = 8L_x$. $N = L_x \times L_y$ is the total number of lattice sites, and the inverse temperature is set to be $\beta = 2 \times \sqrt{N}/J$ for (a) and $\beta = \sqrt{N}/J$ for (b). In (a), $\langle m_s^2 \rangle$ exhibits a minimum for every α_1. When $L_y \gg L_x$, $\langle m_s^2 \rangle$ decreases almost linearly against $1/\sqrt{N}$ in (b). The errors that are visible are of order 10^{-3} and the invisible ones are of 10^{-4} at least.

The correlation lengths will be calculated in the following way:

$$\xi_{\text{zigzag}} = \frac{1}{\delta q_{\text{zigzag}}} \sqrt{\frac{C(\vec{q_0},0)}{C(\vec{q_0}+\vec{\delta q}_{\text{zigzag}},0)} - 1}, \quad (12)$$

$$\xi_\tau = \frac{1}{\omega} \sqrt{\frac{C(\vec{q_0},0)}{C(\vec{q_0},i\omega)} - 1}, \quad (13)$$

where $\vec{q_0} = (0,\pi)$ and $\vec{\delta q}_{\text{zigzag}} = (0,2\pi/L_y)$.

The transverse susceptibility can be calculated by

$$\chi_\perp = \frac{1}{L_x L_y \beta} \left\langle \sum_{j,k} \int_0^\beta d\tau_1 \int_0^\beta d\tau_2 S_j^+(\tau_1) S_k^-(\tau_2) \right\rangle. \quad (14)$$

$\chi_\perp$ would exhibit a divergent behavior at the critical point, and for finite sizes, it shows a power-law behavior,

$$\chi_\perp \propto L^{\gamma/\nu}, \quad (15)$$

where γ is the critical exponent for the susceptibility [33]. We shall employ this quantity to investigate the critical properties induced by staggered fields.

III. CROSSOVER FROM 1D TO 2D

Now let us consider the crossover behavior from 1D to 2D by altering the coupling ratios of the present system. During the calculations, the coupling ratio is changed to the value as low as $\alpha_1 = -0.010$.

We first take L_x and L_y to be equal and the inverse temperature to be size-dependent $\beta = 2\sqrt{N}/J$. Figure 2(a) shows the size extrapolation of m_s^2 versus $1/\sqrt{N}$ for various coupling ratios α. It is seen that as the system size increases, $\langle m_s^2 \rangle$ first decreases and then increases, leaving a minimum at a finite size for each α, and in this case, it shows a nonmonotonic behavior, and therefore a size extrapolation is impossible. It is known that the finite-size gap in the zigzag chain is $\triangle(L_y) \sim \frac{1}{L_y}$. When energy scales in the two directions are compatible, $\triangle(L_y) \sim \rho_x$, where ρ_x scales the energy in the armchair direction, the system crossovers from 1D to 2D [20,21], and in this way, the size extrapolation for the order parameter square is meaningful. In order to make a reasonable size extrapolation, we should take $L_y \gg L_x$ for small $|\alpha_1|$.

We carry out simulations on lattices with $L_y = 8L_x$ for α_1 from −0.04 to −0.18, where the inverse temperature is taken as $\beta = \sqrt{N}/J$. The size extrapolations to the square root of the total number of lattice sites $N = L_x \times L_y$ are shown in Fig. 2(b). It can be observed that $\langle m_s^2 \rangle$ decreases almost linearly against $1/\sqrt{N}$. By doing a polynomial fitting of order two to the data for $\alpha = -0.04$, the size extrapolation of $\langle m_s^2 \rangle$ gives 0.0100(3), suggesting that the system is magnetically ordered.

In Fig. 2(a), the fitting curves for $\alpha_1 = -0.02$ is very close to that for $\alpha_1 = -0.01$ until the thermodynamic limit is reached, where the two curves do not have crossings, implying that the system is in a spin-ordered state when $|\alpha_1|$ is larger than 0.01. The result $\lim_{L\to\infty} \langle m_s^2 \rangle \to 0.0100(3)$ for $\alpha = -0.04$ confirms the above observation. Therefore, on tuning a very small interchain F interaction between the AF zigzag spin chains, the system immediately undergoes a crossover from a disordered 1D state to a 2D spin-ordered state.

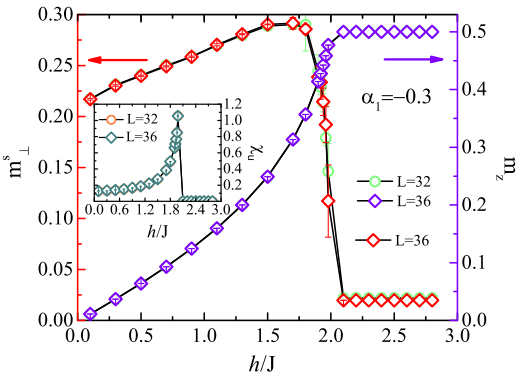

FIG. 3. $m_\perp^s$ m_z and χ_u vs uniform magnetic field h/J for different lattice sizes $L_x = L_y = 32$ with $\beta = 100/J$ and 36 with $\beta = 108/J$ for $\alpha_1 = -0.3$. Inset is the susceptibility χ_u as a function of h/J. Around $h/J = 2$ there is a second-order phase transition between a canted stripe phase and a polarized phase. Except the points whose error bar is visible, the rest of the data are calculated with accuracy of at least 10^{-3}.

IV. MAGNETIZATION IN MAGNETIC FIELDS

We now consider the effects of external uniform and staggered fields on magnetization and susceptibility of the system under interest.

A. Presence of a uniform field

In the presence of a uniform field h, the uniform magnetization m_z, the staggered magnetization in the xy plane $m_\perp^s = \sqrt{\langle m_\perp^2 \rangle}$, and the uniform magnetic susceptibility χ_u have been calculated for $\alpha_1 = -0.3$ on lattices with $L_x = L_y = 32,36$, and $\beta = 100/J$ for $L_x = 32$ and $108/J$ for $L_x = 36$.

Figure 3 shows the field dependence of m_z, $m_\perp^s$, and χ_u for $\alpha_1 = -0.3$. One may see that, in a weak field, m_z increases from zero slowly and goes to saturation when h/J approaches

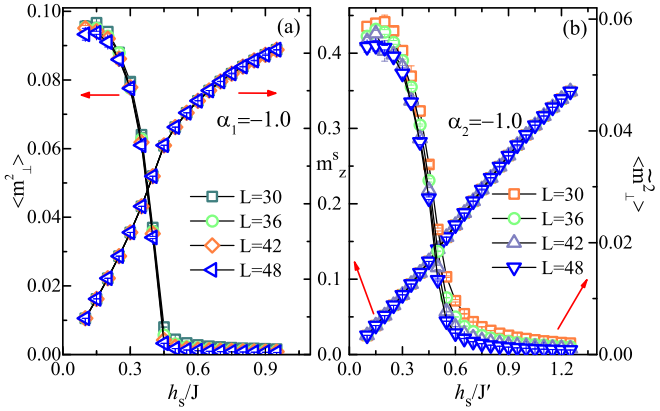

FIG. 4. The transverse staggered magnetization square $\langle m_\perp^2\rangle$ ($\langle \tilde{m}_\perp^2\rangle$) and longitudinal staggered magnetization m_s^z versus the staggered field h_s in the present system with coupling ratio (a) $\alpha_1 = -1.0$ (Case A) and (b) $\alpha_2 = -1.0$ (Case B). Here we take $L_x = L_y = L$. Most of the data are as accurate as 10^{-4}.

to 2.0, while $m_\perp^s$ enhances from a finite value to a peak and then declines sharply around $h/J = 2.0$ and reaches zero when $h/J > 2.0$. The susceptibility χ_u in the inset displays a sharp peak at $h/J = 2.0$, indicating a second-order in-plane phase transition and being consistent with the observation in magnetic curves. When h is applied, the z component (out-of-plane component) of magnetic moments begins to develop with the decay of the in-plane $m_\perp^s$; when $h/J \geqslant 2$, the system is fully polarized and the transverse component is totally suppressed. We call such a phase before fully polarized the canted stripe phase, in which $m_\perp^s > 0$ and $m_z > 0$.

In contrast, for the system considered in Ref. [24] where $J < 0$ and $J' > 0$, there is a phase transition at $\alpha_2 = \frac{J}{J'} \simeq -0.93$ from a disorder dimer phase to an ordered stripe phase, where the spin alignments are parallel along the same zigzag line and antiparallel along the armchair direction. m_z, $\tilde{m}_\perp^s$ (the staggered magnetization in xy plane for the system explored in Ref. [24]) and χ for the ordered phase look like the ones of this present system. When it is in the dimer phase for $\alpha_2 = -0.6$, the zero magnetization plateau appears in m_z, $\tilde{m}_\perp^s$, and χ. Since the present system has an in-plane long-range order ($m_\perp^s \neq 0$) in the ground state, the excitation is gapless with Goldstone bosons, and there is no zero magnetization plateau in the magnetic curve (Fig. 3).

B. Presence of a staggered field

In this subsection, we shall investigate the magnetic curves in the present system (Case A) and the system discussed in Ref. [24] (Case B) in a staggered field h_s (while keeping $h = 0$). We study the staggered magnetization m_z^s [Eq. (9)] and the magnetization square in the xy plane $\langle m_\perp^2\rangle$ under a field h_s for $\alpha_1 = -1.0$ and $\langle \tilde{m}_\perp^2\rangle$ for $\alpha_2 = -1.0$, respectively. The simulations are performed on lattices with $L_x = L_y = 30$, 36, 42, 48 and $\beta = 100/J(J')$ for $L_x < 30$ and $3 \times L_x/J(J')$ for $L_x > 34$.

Figure 4 presents the transverse staggered magnetization square $\langle m_\perp^2\rangle$ ($\langle \tilde{m}_\perp^2\rangle$) and longitudinal staggered magnetization m_s^z as a function of staggered field $h_s/J(J')$ of the system for $\alpha_1 = -1.0$ [Case A in Fig. 4(a)] and $\alpha_2 = -1.0$ [Case B in Fig. 4(b)], where both are spin ordered in the ground state in the absence of a magnetic field. It is observed that for both cases, with increasing the staggered magnetic field, $\langle m_\perp^2\rangle$ ($\langle \tilde{m}_\perp^2\rangle$) decreases from a finite value (around 0.1 for Case A and 0.06 for Case B) to sharply vanishing at a critical field $h_s/J \simeq 0.45$ and $h_s/J' \simeq 0.50$ for Case A and Case B, respectively, where the in-plane QPT at critical fields appears to be of second order, while m_s^z increases almost linearly in the region of weak fields. This is understandable, as the staggered magnetic field is applied along the z (out-of-plane) direction, with the increase of the field, the transverse magnetization in the xy plane will be gradually suppressed, while the longitudinal magnetization grows until saturation, as manifested in Fig. 4. Recall that in the absence of an external field, the system with mixing F and AF bond couplings has a spin-ordered ground state.

For the two cases, the behaviors of $\langle m_\perp^2\rangle$ and $\langle \tilde{m}_\perp^2\rangle$ look qualitatively similar, but the in-plane critical fields differ somewhat; m_s^z behaviors slightly in a different way: Case A goes to magnetic saturation faster than Case B, because the former can be viewed as the antiferromagnetic zigzag spin chains coupled ferromagnetically, whereas the latter is formed by ferromagnetic zigzag spin chains coupled antiferromagnetically. In addition, the finite-size effect in Case B appears to be more obvious than in Case A.

V. SCALING BEHAVIOR IN A STAGGERED FIELD

Binder ratios [34–36] and spin stiffness [28] are proper quantities for investigating the critical features of the system. As h_s breaks the O(3) spin rotating symmetry, and the in-plane order parameter disappears at the critical point, we consider only the spin stiffness ρ for simplicity. As mentioned in Sec. III, ρ could be directly related to the superfluid density of a superconductor or superfluid [29,30,37,38], marking the occurrence of off-diagonal long-range order. According to the previous study [39], at the critical point it scales as $\rho \sim L^{2-d-z}$, where d is the spatial dimension of the system, and z is the dynamical exponent. Here we set z as 1 (we would prove it later) and measure ρL which is size independent at the critical point.

For Case A with $\alpha_1 = -1.0$, a staggered field h_s/J in [0.4145, 0.435] has been applied to the system on lattices $L_x = L_y = 20$, 24, 28, 32, 36, 40, 44, and 48 with $\beta = 100/J$ for $L_x < 34$ and $3L_x/J$ for $L_x > 34$. Figures 5(a) and 5(c) present the field dependence of $\rho_x L_x$ and $\rho_y L_y$, showing that the curves for different lattice sizes do intersect at about 0.424, which must be a critical point. To confirm this, we perform a finite-size scaling (FSS) by making a data collapse analysis, as shown in Figs. 5(b) and 5(d), where all curves fall on a single almost-straight line (see below for details).

For Case B with $\alpha_2 = -1.0$, we calculate $\rho_x L_x$ and $\rho_y L_y$ as a function of a staggered magnetic field on lattice sizes from $L = 12$ to $L = 42$ with $\beta = 100/J'$ for $L_x < 34$ and $3L_x/J'$ for $L_x > 34$, as shown in Figs. 6(a) and 6(c), from which one may see that there is a crossing point at about $h_s/J' \simeq 0.495$, demonstrating that it may be a quantum critical point. The corresponding data collapses confirm this observation that all curves for different lattice sizes go to a single line [Figs. 6(b) and 6(d)]. It is also consistent with the vanishing points for

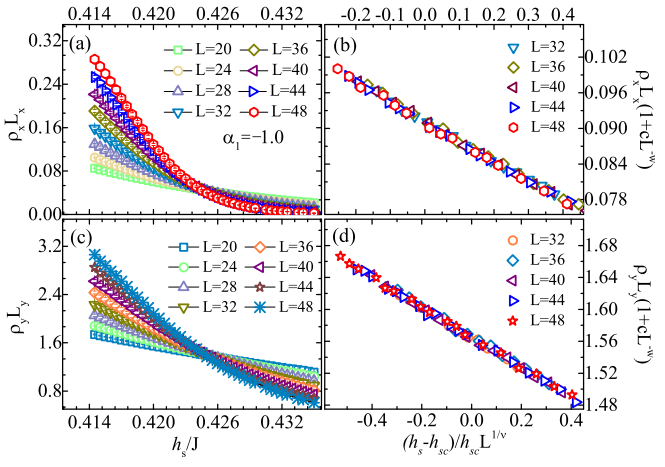

FIG. 5. (a) $\rho_x L_x$ and (c) $\rho_y L_y$ as function of h_s/J of the system with coupling ratio $\alpha_1 = -1.0$ near the critical point for various lattice sizes $L = 20, 24, 28, 32, 36, 40, 44$, and 48; panels (b) and (d) are the corresponding data collapses for the finite-size scaling, where the data fall on a line, respectively, giving a critical staggered field $h_{sc}/J \simeq 0.42373(4)$ and an exponent $\nu = 0.677(2)$, which indicates that this may be an O(3) universality transition. The errors for ρ_x are mostly of 10^{-4} and for ρ_y of 10^{-3}.

$\langle \tilde{m}_\perp^2 \rangle$ shown in Fig. 4, confirming the second-order QPT triggered by a staggered field. Here we would like to point out that in Ref. [24] we discussed the scaling behaviors of $\rho_x L_x$ and $\rho_y L_y$ against the coupling ratio (here $|\alpha_2|$), where the QPT occurs at a critical coupling ratio, and the transition induced by the staggered magnetic field is left for our present study.

In the framework of the renormalization group, the finite-size scaling plays as an essential role in studying the critical behavior near the transition point in finite-size systems [27,40–42]. In the vicinity of a critical point, the correlation

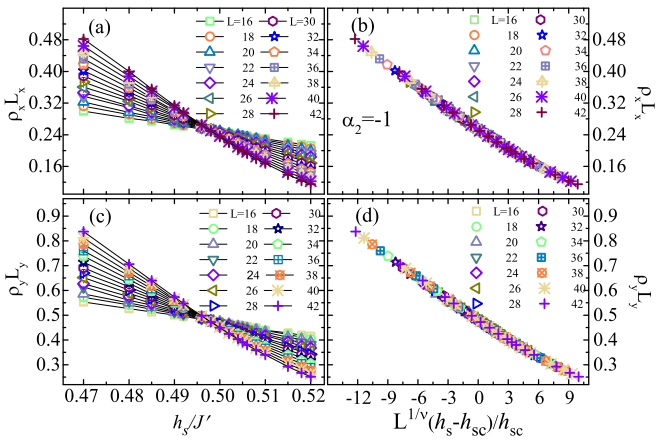

FIG. 6. (a) $\rho_x L_x$ and (c) $\rho_y L_y$ as function of h_s/J' of the system considered in Ref. [24] with $\alpha_2 = -1.0$ for various lattice sizes from $L = 16$ to 42, where a crossing point is seen at the staggered field $h_s/J' \simeq 0.495$; panels (b) and (d) show the corresponding data collapse for the FSS fit, which gives $h_{sc}/J' \simeq 0.497266(3)$ and $\nu \simeq 0.6947(2)$. This result along with $\nu = 0.7086(3)$ for lattice sizes of $L = 24 \sim 42$ indicates that this QPT belongs to the classical Heisenberg O(3) universality. The errors are at least 10^{-3}.

TABLE I. The critical staggered magnetic field h_{sc}, the exponent ν of correlation length in Case B for different sets of lattice sizes and the respective χ^2/DOF.

		h_{sc}/J'	ν	χ^2/DOF
$\rho_x L_x$	$L = 14 \sim 36$	0.49997(2)	0.661(1)	15.3912
	$L = 16 \sim 42$	0.497483(3)	0.6982(3)	3.6933
	$L = 24 \sim 42$	0.496974(6)	0.7112(4)	3.57886
$\rho_y L_y$	$L = 14 \sim 36$	0.49883(2)	0.667(1)	11.5542
	$L = 16 \sim 42$	0.497266(3)	0.6947(2)	2.9307
	$L = 24 \sim 42$	0.496884(4)	0.7086(3)	2.76738

length ξ is divergent and, as the lattice size obeys $L \leqslant \xi$, some quantities exhibit power-law divergent behaviors with ξ and could be expressed by a scaling function of the form $Q(t,L) = L^{\kappa/\nu} g(tL^{1/\nu})$, where κ is the critical exponent of Q and ν of ξ, t is the reduced phase transition tuning parameter, and $g(x)$ is a smooth function which asymptotically behaves as $g(x) \sim x^{-\kappa}$ for $x \to \infty$. Here for ρL, κ is zero and $t = (h_s - h_{sc})/h_{sc}$.

In Case A, the intersection points for different pairs $[L, L']$, where $L' > L$, shift as L enlarges, and a general scaling function under such conditions with extra corrections to $tL^{1/\nu}$ and $Q(t,L)$ [43] can be taken,

$$(1 + cL^{-\omega})Q(t,L) = g(tL^{1/\nu} + dL^{-\phi}). \tag{16}$$

The following scaling form will be more convenient:

$$(1 + cL^{-\omega})Q(t,L) = a_0 + a_1 tL^{1/\nu} + a_2 (tL^{1/\nu})^2, \tag{17}$$

where c, ω, a_0, a_1, and a_2 are constants to be determined. For Case A only the correction $(1 + cL^{-\omega})$ [23] for $\rho_{x(y)} L_{x(y)}$ is included in the scaling functions.

For Case B, the form $Q(t,L) = L^{\kappa/\nu} g(tL^{1/\nu})$ works very well, and the scaling function is supposed to be polynomial of order two:

$$Q'(t,L) = a_0' + a_1' tL^{1/\nu} + a_2' (tL^{1/\nu})^2, \tag{18}$$

where a_0', a_1', a_2', and ν are constants independent of L.

The data are analyzed following the lines in Ref. [39]. We take thousands of copies of bootstrap resamplings of the raw data as the fitting data and prepare the same amount of sets of initial fitting parameters in the above functions as the input in fitting procedures, which are based on the nonlinear Levenberg-Marquardt optimization algorithm (LMOA) [44]. For Case A, h_s/J in the interval of [0.4230, 0.4245] for lattice sizes $L_x = L_y = 32,36,40,44,48$ is taken in the optimization procedure, while for Case B, all the data in Figs. 6(a) and 6(c) are considered. The corresponding collapsed curves are shown in Figs. 5(b) and 5(d) and then Figs. 6(b) and 6(d), respectively.

Based on the criteria of the lowest χ^2/DOF [e.g., the weighted sum of squares residual per degree of freedom (DOF)] for each single LMOA fitting, in Case B, it gives $h_{sc}/J' = 0.497266(3)$ and $\nu = 0.6947(2)$. We also checked the size effect [45] on the scaling by doing the finite-size scaling on lattices of $L = 14$, 16, 18, ..., 36 and $L = 24$, 26, 28, ..., 42, respectively. The corresponding fitting results are shown in Table I. The lowest χ^2/DOF in $\rho_y L_y$ for $L = 24 \sim 42$ gives $\nu \simeq 0.7086(3)$ and $h_{sc}/J' \simeq 0.496884(4)$.

The exponent ν for case B is close to $\nu = 0.7112(5)$ [33], showing that its QPT belongs to the classical Heisenberg O(3) universality; while for Case A, it gives $h_{sc}/J = 0.42373(4)$ and $\nu = 0.677(2)$, showing that ν lies in the interval of [0.67155(27), 0.7112(5)], where $\nu = 0.67155(27)$ is the 3D xy universality [46]. To determine the type of universality, in the following we utilize another method in Ref. [32] to study the exponent for Case A.

For the finite-size lattices at the critical point, the correlation length ξ_θ would scale monotonically to the lattice width L_θ at θ direction in the real space or in the imaginary time axis [28,32]:

$$\xi_\theta/L_\theta = \tilde{\xi}_\theta(tL^{1/\nu}, L^z/\beta), \tag{19}$$

where $\tilde{\xi}_\theta$ is an asymptotic scaling function of $tL^{1/\nu}$ and L^z/β. As mentioned above, the correlation length ξ_θ diverges with the reduced staggered field, $|t| \sim \xi_\theta^{-1/\nu}$, and $\xi_\tau \sim L^z$. When tuning the staggered field h_s and the imaginary time β to keep $\tilde{\xi}_\theta = R_\theta$ constant, the size-dependent critical point $h_{sc}(L)$ and the corresponding $\beta(L)$ scales with lattice width L as

$$h_{sc}(L) - h_{sc} \sim L^{-1/\nu} \tag{20}$$

and

$$\beta(L) \sim L^z. \tag{21}$$

The following relation holds:

$$h_{sc}(R,L) = h_{sc} + c(R)L^{-1/\nu}. \tag{22}$$

The Robbins-Monro stochastic (RMS) approximation method [32] is applied to the iterative tuning process for $h_{sc}(R,L)$ and $\beta(L)$. For each set of (L,R), hundreds of $h_{sc}(L,R)$ and $\beta_{L,R}$ convergence are achieved. For Case A, we carried out simulations for $R_{\text{zigzag}} = R_\tau = R = 0.3$, 0.4, and 0.5 on lattices with $L_x = L_y = 24,28,32,\ldots,100$. Here thousands of bootstrap resampling of raw data were also performed for the LMOA fitting procedures with data of $L_x = L_y \geqslant 40$, and each R is supposed to share the same h_{sc} and ν.

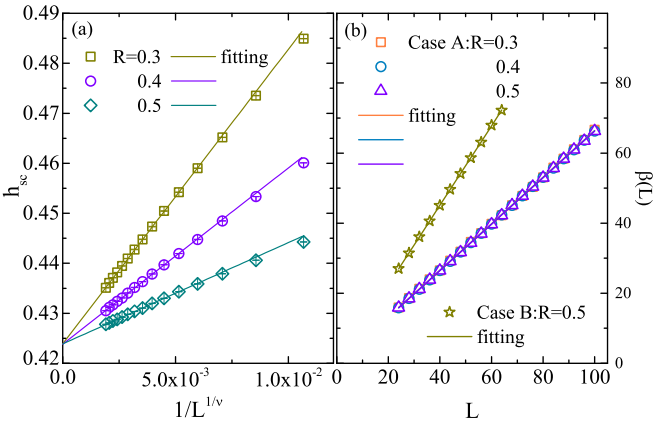

FIG. 7. (a) $h_{sc}(L) \sim 1/L^{1/\nu}$ curves at constant ratios of $R = 0.3$, 0.4 and 0.5 in Case A for $L = 24,28,\ldots,100$; (b) $\beta(L) \sim L$ at different ratios R for Case A and $R = 0.5$ for Case B. Solid lines indicate the fittings of data. Curves in (a) share the same exponent ν and h_{sc}, and thousands of LMOA fittings give $\nu = 0.70046(1)$ and $h_{sc} = 0.423831(2)$. $\beta(L)$ increases linearly with the lattice size, indicating that the exponent z is 1.

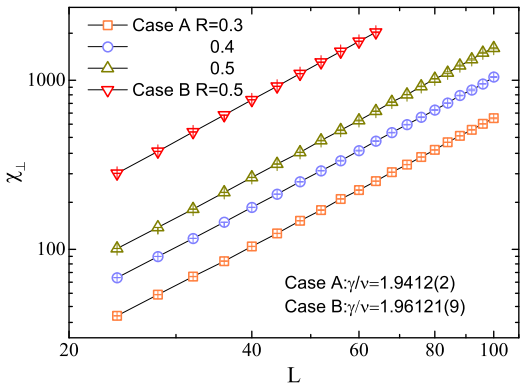

FIG. 8. The size-dependent transverse susceptibility $\chi_\perp$ at different ratios R for Case A with $\alpha_1 = -1.0$ and Case B with $\alpha_2 = -1.0$ in logarithmic plots. The curves behavior linearly, and the slopes are fitted to be 1.9412(2) for Case A and 1.96121(9) for Case B.

h_{sc}, ν, and z are fitted to be 0.423831(2), 0.70046(1) [47], and 1.006572(9), respectively, and χ^2/DOF is about 1.5. For Case B, we applied the calculations on lattices with $L_x = L_y = 24$, 28, 32, . . . , 64, and the dynamic exponent z is fitted to be about 1.004615(8). So the assumption of $z = 1$ in calculations of ρL is reasonable. Considering the lowest χ^2 and large-enough lattice sizes, the correlation length exponent ν for Case A can be determined to be 0.70046(1), showing that the quantum phase transition is also of Heisenberg O(3) universality.

Figure 7 presents the curves of $h_{sc}(R,L) \sim L^{-1/\nu}$ at different R for Case A and $\beta(L)L$ at the same ratios R in Case A and $R = 0.5$ for Case B. The fitting results show that the raw data are scaled quite well by the scaling functions with proper parameters.

In addition, we also calculated the transverse susceptibility $\chi_\perp$ at each of critical points $h_{sc}(R,L)$ gained by RMS method for Case A and Case B. Along with the resamplings mentioned above, $\chi_\perp$ is prepared with thousands of copies in the fitting procedures. For a finite-size system, $\chi_\perp \propto L^{\gamma/\nu}$. We plot the $\chi_\perp \sim L$ curves in logarithmic plots, as shown in Fig. 8, which shows that the curves behavior linearly and the slopes are obtained to be 1.9412(2) for Case A and 1.96121(9) for Case B, respectively.

Table II presents the critical staggered magnetic field h_{sc}, the exponent ν of correlation length, the dynamic exponent z, and γ/ν of susceptibility for both cases.

VI. PHASE DIAGRAM IN A STAGGERED FIELD

As shown in Fig. 4, when $h_s < h_{sc}$ both systems exhibit a staggered magnetization in the z direction and keep the corresponding stripe order in the xy plane, that is, $m_z^s > 0$ and $\langle m_\perp^2 \rangle (\langle \tilde{m}_\perp^2 \rangle) > 0$. We coin the so-defined phase for $h_s < h_{sc}$ as the canted phase I for Case A and the canted phase II for Case B. As $h_s > h_{sc}$, only the out-of-plane staggered magnetization remains in both cases, say, $m_z^s > 0$, and $\langle m_\perp^2 \rangle (\langle \tilde{m}_\perp^2 \rangle) = 0$. We call such a phase for $h_s > h_{sc}$ the Néel phase in a staggered field.

To draw a phase diagram, we inspect various coupling ratios for the two cases and make use of the transition points in the curves of m_z^s, $\langle m_\perp^2 \rangle$, $\langle \tilde{m}_\perp^2 \rangle$, and ρL vs h_s for each α_1 or α_2,

TABLE II. The critical staggered magnetic field h_{sc}, the exponent ν of correlation length, the dynamic exponent z, and the exponent γ/ν of susceptibility are determined for the present system (Case A) and the system (Case B) considered in Ref. [24].

		$h_{sc}/J(J')$	ν	z	γ/ν
Case A	$\rho_x L_x$	0.4233(1)	0.686(3)	—	—
	$\rho_y L_y$	0.42373(4)	0.677(2)	—	—
	RMS	0.423831(2)	0.70046(1)	1.006572(9)	1.9412(2)
Case B	$\rho_x L_x$	0.496974(6)	0.7112(4)	—	—
	$\rho_y L_y$	0.496884(4)	0.7086(3)	—	—
$L = 24 \sim 42$	RMS	—	—	1.004615(8)	1.96121(9)

forming the phase boundaries. In doing so, a schematic phase diagram in the plane of $h_s/J(J')$ vs $-\alpha_{1(2)}$ is thus depicted in Fig. 9.

For Case A, as shown in Fig. 9(a), there are three phases, the stripe phase I (where $m_z^s = 0$ but $\langle m_\perp^2 \rangle > 0$), the canted phase I, and the Néel phase. The stripe phase I always remains in the absence of a staggered field. When h_s is increasing, the system immediately first enters the canted phase I and then enters the Néel phase when $h_s > h_{sc}$.

For Case B, as shown in Fig. 9(b), there are four phases, a dimerized phase, the stripe phase II, the canted phase II, and the Néel phase. Our previous study [24] shows that in the absence of a magnetic field, there is a phase transition at the critical point $\alpha_{2c} \simeq -0.93$ from a dimer phase to a stripe phase II with a nonvanishing $\langle \tilde{m}^2 \rangle = \frac{3}{2}\langle \tilde{m}_\perp^2 \rangle$ but $m_z^s = 0$. When the staggered field is increasing, the system in Case B immediately enters the Néel phase for $-\alpha < -\alpha_2$, while for $-\alpha > -\alpha_2$, the system first enters the canted phase II (where $m_z^s > 0$ and $\langle \tilde{m}^2 \rangle > 0$), and then enters the Néel phase ($m_z^s > 0$ but $\langle \tilde{m}^2 \rangle = 0$) when $h_s > h_{sc}$.

VII. TEMPERATURE DEPENDENCE OF SUSCEPTIBILITY AND SPECIFIC HEAT IN MAGNETIC FIELDS

In this section, we study the temperature dependence of the susceptibility χ_u and specific heat C_v under different magnetic fields. The results are given in Figs. 10, 11, and 12, respectively. The simulations were carried out on lattices with $L_x = L_y = 30$.

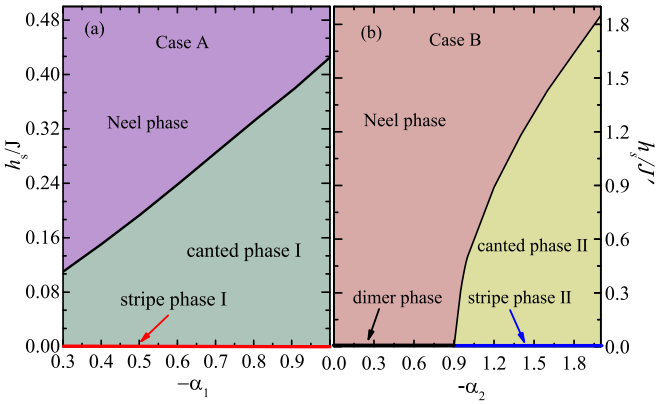

FIG. 9. Phase diagram for the present system (Case A) and the system (Case B) considered in Ref. [24] in the plane of the coupling ratio $\alpha_{1,2}$ versus staggered magnetic field h_s.

In subsection IVA, it shows that for $\alpha_1 = -0.3$ the system is polarized when $h/J \geqslant 2.0$, and when $h/J < 2.0$, the system stays in a canted stripe state with $m_\perp^s > 0$ and $m_z > 0$. In Fig. 10, one may see that for $h/J < 2.0$, χ_u increases from a finite value with increasing temperature, which becomes larger with the increase of the magnetic field, and after undergoing a maximum it decreases quickly at low temperature; when h gets higher, the peak is sharper; as h is close to the critical point, χ_u decays almost exponentially. When $h/J = 2.0$, χ_u diverges as T decreases. For $h/J > 2.0$, $\chi_u(T)$ is suppressed by the magnetic field, leading to all curves being below those of $h/J <= 2.0$, showing that the system enters a different state. At high temperature, all curves coincide with each other due to the domination of thermal fluctuations. At low temperature, when the system is partially polarized, χ_u is influenced mainly by the transverse quantum fluctuations in the xy plane and, closer to the critical point, the stronger the quantum fluctuations and higher χ_u.

Figure 11 shows the temperature dependence of the specific heat C_v of the system with $\alpha_1 = -0.3$ under uniform fields. It can be observed that besides a round peak as that for

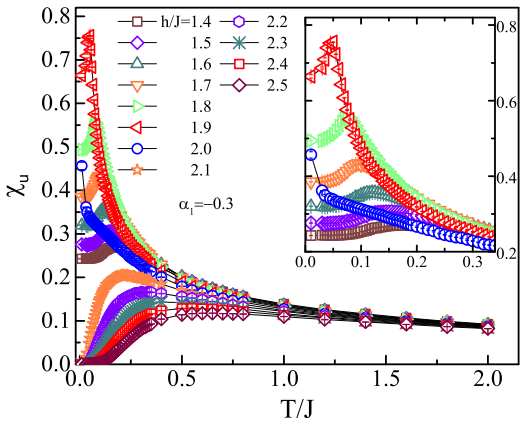

FIG. 10. Temperature dependence of the susceptibility χ_u of the system with $\alpha_1 = -0.3$ under various uniform magnetic fields. The inset shows $\chi_u(T)$ for $h < h_c$ and $T/J < 0.34$. χ_u behaves differently in a low-temperature region: When $h/J < 2.0$, χ_u first goes to sharp peaks and then decreases quickly; when $h/J = 2.0$, χ_u diverges as T/J decreases, characterizing a critical point; and when $h/J > 2.0$, χ_u starts from a vanishing point at $T/J = 0$ and forms a round peak. We find that as $h_c - h > 0$ gets smaller, the peaks of χ_u get larger at small temperatures, and at a given temperature, $\chi_u(h < h_c) > \chi_u(h > h_c)$. The accuracy here is as small as 10^{-4}.

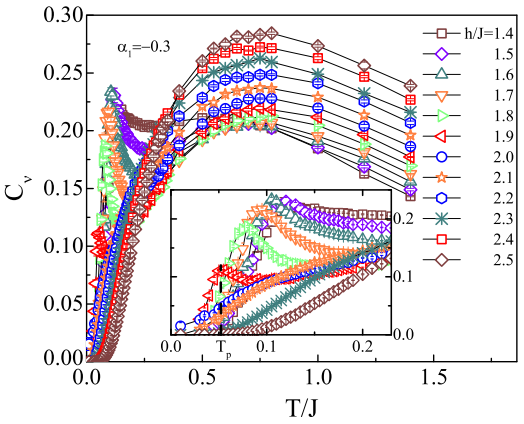

FIG. 11. Temperature dependence of specific heat C_v for the system with $\alpha_1 = -0.3$ under different uniform fields. The inset is the low-temperature part. Before the system is polarized, C_v exhibits an extra peak at low temperature besides the round peak at relatively high temperature. Errors here are of 10^{-3}, and the system size is set to be $L_x = L_y = 30$.

$h/J > 2.0$, in the range of $1.4 < h/J < 2.0$, C_v exhibits a sharp peak at a lower temperature T_p, as shown in the inset of Fig. 11. When h increases, T_p and $C_v(T_p)$ decrease. This could be understood in the following way. As indicated in Fig. 1, the spins along the zigzag chain form a continuous antiferromagnetic arrangement, dividing the system into two sublattices and producing two sets of degenerate spin-wave spectra: $\hbar\omega_k = f(J,J',S,\gamma_k)$, where S is the spin on each site, and γ_k is the static structure factor. A uniform field h would split this overlapping spectra with a shift, $\hbar\omega_k^{\pm} = f(J,J',S,\gamma_k) \pm h$, resulting in that two modes of low-lying excitations cause two minimums [48,49] in C_v. The part of C_v contributed by the lower-frequency mode increases faster. h enlarges the difference of the increasing tendency between $\hbar\omega_k^+$ and $\hbar\omega_k^-$, making C_v steeper and T_p smaller for larger $h < h_c$ at low temperature. When $h > h_c$, the system enters the polarized state, and C_v versus T/J exhibit only one round peak at a relatively higher temperature.

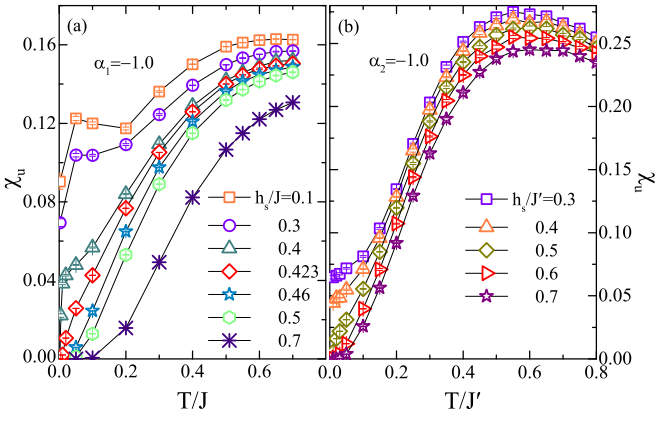

FIG. 12. Temperature dependence of susceptibility χ_u of the system with (a) $\alpha_1 = -1.0$ and (b) $\alpha_2 = -1.0$ under various staggered magnetic fields. The order for the error bars are 10^{-3}. The lattice size is $L_x = L_y = 30$.

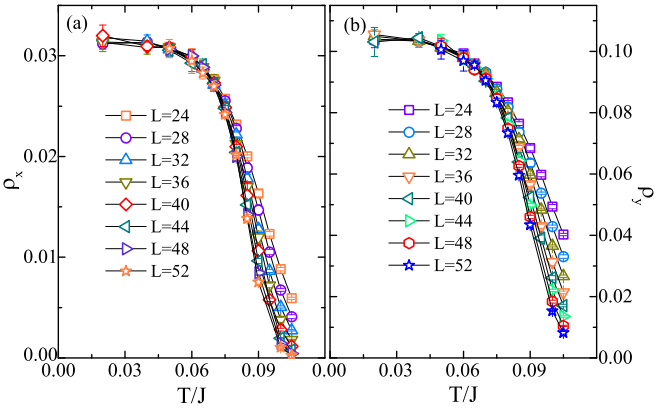

FIG. 13. Finite-temperature spin stiffness (a) ρ_x and (b) ρ_y of the present system with $\alpha_1 = -1.0$ under a uniform field $h_u = 1.8J$ on lattices with $L_x = 24,28,\ldots,52$. The errors for most of the data are of scale 10^{-4}. As T is larger than around 0.06, both ρ_x and ρ_y decrease rapidly for larger sizes, indicating that a KT phase transition occurs.

In Fig. 12, it depicts the temperature dependence of susceptibility χ_u for systems with $\alpha_1 = -1.0$ and $\alpha_2 = -1.0$ under different staggered magnetic fields, which differ from those in a uniform magnetic field. We showed that a staggered field can induce a quantum phase transition in Sec. V, which eliminates the off-diagonal long-range order in the xy plane at $h_{sc}/J \simeq 0.423$ for $\alpha_1 = -1.0$ and $h_{sc}/J' \simeq 0.5$ for $\alpha_2 = -1.0$. Figures 12(a) and 12(b) illustrate that, as $h_s < h_{sc}$, χ_u would start from a nonvanishing value, while, as $h_s \geqslant h_{sc}$, the susceptibility χ_u goes to zero at $T \to 0$, revealing that the system in this situation enters distinct phases under different staggered magnetic fields, consistent with the observation in Fig. 9.

VIII. FINITE-TEMPERATURE KOSTERLITZ-THOULESS PHASE TRANSITION IN A UNIFORM FIELD

The Kosterlitz-Thouless (KT) transition at a critical temperature $T_{\rm KT}$ happens when the vortex-antivortex pairs are unbounded by thermal fluctuations without breaking any symmetry of the original system [50]. As $T < T_{\rm KT}$, the correlation function with a power-law decay maintains a nonzero spin stiffness with a weaker finite-size effect, and when $T > T_{\rm KT}$, $\rho(T,L)$ shows a discontinuity to zero as L increases. For $\alpha_1 = -1.0$ under a uniform field $h_u = 1.8J$ at finite temperature, we measured the spin stiffness ρ_x and ρ_y on lattices of different sizes. We found that there is indeed a KT phase transition by observing that, when temperature T increases, $\rho_{x(y)}$ drops from a finite value to vanishing. As the lattice size $L_x = L_y = L$ increases, such a rapid decrease is more obvious.

Figure 13 presents the results of ρ_x and ρ_y at finite temperature of the present system with $\alpha_1 = -1.0$ under a uniform field for different lattice sizes. At low temperature, $\rho_{x(y)}$ decreases slowly with the increase of T, and when T is larger than about $0.06J$, $\rho_{x(y)}$ drops rapidly to zero, demonstrating that a KT phase transition might happen at temperature $T_{\rm KT} \approx 0.06J$. Instead of the methods introduced in Ref. [37] or Ref. [51], we here deal with the scaling relation

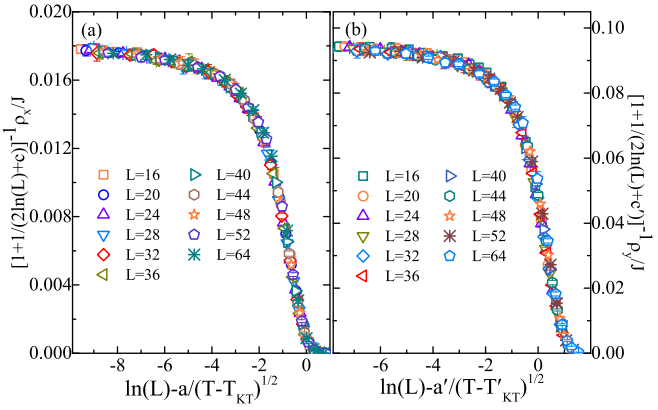

FIG. 14. Data collapse with trial parameters for ρ_x and ρ_y according to the scaling relation between $[\ln(L) - a/(T - T_{\rm KB})^{1/2}]$ and $\rho_{x(y)}[1 + \frac{1}{2\times\ln(L)+c}]^{-1}$. All curves collapse onto a single curve for both ρ_x and ρ_y. Because of the anisotropy of the lattice, $\rho_x(T,L) \neq \rho_y(T,L)$ and the fitted parameters differ.

of $[\ln(L) - a/(T - T_{\rm KB})^{1/2}] \sim \rho_{x(y)}[1 + \frac{1}{2\times\ln(L)+c}]^{-1}$ directly and tune the parameters a, T_{KB}, c to make all data for $T \geqslant 0.066$ to collapse onto one curve as much as possible. Figure 14 shows the collapsed curves with the suitable parameters. For ρ_x, a and c are about 0.75 and 0.6, respectively, and a' and c' are 0.63 and 0 for ρ_y. $T_{\rm KT}$ for both ρ_x and ρ_y is about $0.0623J$. By combining the facts of the rapid dropping behaviors of ρ_x and ρ_y and the corresponding data collapse onto one single curve for both ρ_x and ρ_y, we believe that the KT phase transition occurs at about $T_{\rm KT} \cong 0.0623J$.

IX. SUMMARY

The spin-1/2 Heisenberg model with AF and F mixing interactions on a honeycomb lattice has been studied by means of the continuous imaginary-time QMC with the worm update algorithm in uniform and staggered magnetic fields. It is found that so long as the F coupling on armchair bonds is tuned, the system (Case A) immediately crosses over smoothly from 1D disordered AF zigzag spin chains to a stripe-ordered 2D phase with $\langle m_s^2 \rangle > 0$. This is in contrast to the system considered in Ref. [24] where the F interactions are presumed on zigzag bonds and AF interactions on armchair bonds. In this latter system (Case B), on tuning the F interactions on zigzag bonds, the system shows a phase transition from a disordered dimerized phase to a stripe-ordered 2D phase.

In the presence of uniform or staggered magnetic fields, it is shown that for a given coupling ratio (e.g., $\alpha_1 = -0.3$ in a uniform field and $\alpha_{1,2} = -1.0$ in a staggered field), with increasing the external magnetic fields, the system enters smoothly into a spin-canted phase from a stripe-ordered phase and then undergoes a QPT into an out-of-plane polarized phase or Néel phase. This is also true for the system in Case B for the coupling ratio beyond a critical value (satisfying $-\alpha_2 > 0.93$). The whole phase diagrams in the plane of coupling ratio and staggered magnetic field for the systems in Case A and Case B are obtained. In Case A, there are three phases, including a stripe-ordered phase, a canted phase, and a Néel phase, while in Case B, there are four phases, say, the dimerized phase, stripe phase, canted phase, and Néel phase.

In addition, by exploring the spin stiffness, the scaling behaviors in a staggered field for both systems are also discussed. The finite-size scaling analysis gives that the exponent ν of correlation length is 0.7086(3) for Case B, and the Robbins-Monro method gives $\nu = 0.70046(1)$ for Case A, both of which are close to $\nu = 0.7112$ of the classical Heisenberg O(3) universality, indicating that both systems fall into the O(3) universality. Besides, the scaling functions differ from the two systems. The dynamic exponent z for Case A and Case B are calculated to be 1.006572(9) and 1.004615(8), respectively, confirming the reliability of the assumption of $z = 1$ when calculating ρL in scaling analysis.

The temperature dependence of susceptibility χ_u and specific heat C_v have been studied for the system with $\alpha_1 = -0.3$ under various uniform fields. When the system stays in the canted stripe phase as $h/J < 2.0$, at low temperature the partially polarized spins have a nonzero value of χ_u in the ground state and a sharp peak of $\chi_u(T)$ appears at low temperature; meanwhile, the specific heat C_v also presents a sharp peak starting from a vanishing value when $T/J \to 0$. As $h/J \geqslant 2.0$, the polarized ferromagnetic state does not display such features because of nondegenerate spin-wave spectra which could be separated by the uniform magnetic field. The behaviors of χ_u versus $T/J(J')$ for $\alpha_1 = -1.0$ and $\alpha_2 = -1.0$ under different staggered fields are consistent with the phase diagram presented in Sec. V. Through measuring the spin stiffness for $\alpha_1 = -1.0$ under a uniform field $h_u = 1.8J$ at finite temperature, a KT phase transition is discovered at temperature $T_{\rm KT} \approx 0.0623J$.

The present study shows that the competition among mixing interactions, external probes such as staggered magnetic field and temperature, as well as the topology of the lattice together result in more complex phenomena in quantum many-body systems. Our results would also be helpful for further understanding the physical properties and scaling behaviors in 2D magnetic materials with mixing AF and F interactions.

ACKNOWLEDGMENTS

The authors acknowledge W. Li, B. Xin, X. Yan, and Z. C. Wang for helpful discussions. This work was supported in part by the MOST of China (Grant No. 2013CB933401), the NSFC (Grant No. 11474279), and the Strategic Priority Research Program of the Chinese Academy of Sciences (Grant No. XDB07010100).

[1] S. Yan, D. A. Huse, and S. R. White, Science **332**, 1173 (2011).

[2] S. Depenbrock, I. P. McCulloch, and U. Schollwöck, Phys. Rev. Lett. **109**, 067201 (2012).

[3] T.-H. Han, J. S. Helton, S. Chu, D. G. Nocera, J. A. Rodriguez-Rivera, C. Broholm, and Y. S. Lee, Nature **492**, 406 (2012).

[4] Y. Iqbal, F. Becca, S. Sorella, and D. Poilblanc, Phys. Rev. B **87**, 060405(R) (2013).

[5] Z. Y. Xie, J. Chen, J. F. Yu, X. Kong, B. Normand, and T. Xiang, Phys. Rev. X **4**, 011025 (2014).

[6] T. Liu, S.-J. Ran, W. Li, X. Yan, Y. Zhao, and G. Su, Phys. Rev. B **89**, 054426 (2014).

[7] T. Liu, W. Li, A. Weichselbaum, J. von Delft, and G. Su, Phys. Rev. B **91**, 060403(R) (2015).

[8] T. Liu, W. Li, and G. Su, Phys. Rev. E **94**, 032114 (2016).

[9] A. W. Sandvik, Phys. Rev. Lett. **98**, 227202 (2007).

[10] K. J. Runge, Phys. Rev. B **45**, 7229 (1992); **45**, 12292 (1992); N. Trivedi and D. M. Ceperley, *ibid.* **41**, 4552 (1990).

[11] T. Oguchi, Phys. Rev. **117**, 117 (1960).

[12] K. Kojima, M. Larkin, B. Nachumi, Y. Uemura, H. Eisaki, M. Motoyama, S. Uchida, B. Sternlieb, and G. Shirane, Czech. J. Phys. **46**, 1945 (1996); K. Yamada, J. Wada, S. Hosoya, Y. Endoh, S. Noguchi, S. Kawamata, and K. Okuda, Physica C **253**, 135 (1995); K. M. Kojima, Y. Fudamoto, M. Larkin, G. M. Luke, J. Merrin, B. Nachumi, Y. J. Uemura, N. Motoyama, H. Eisaki, S. Uchida, K. Yamada, Y. Endoh, S. Hosoya, B. J. Sternlieb, and G. Shirane, Phys. Rev. Lett. **78**, 1787 (1997).

[13] T. Sakai and M. Takahashi, J. Phys. Soc. Jpn. **58**, 3131 (1989).

[14] A. H. Castro Néto and D. Hone, Phys. Rev. Lett. **76**, 2165 (1996); D. Hone and A. H. Catro Néto, J. Suppercond. **10**, 349 (1997).

[15] I. Affleck, M. P. Gelfand, and R. R. P. Singh, J. Phys. A **27**, 7313 (1995).

[16] T. Aoki, J. Phys. Soc, Jpn. **64**, 605 (1994).

[17] D. Ihle, C. Schindelin, A. Weisse, and H. Fehske, Phys. Rev. B **60**, 9240 (1999); A. Parola, S. Sorella, and Q. F. Zhong, Phys. Rev. Lett. **71**, 4393 (1993).

[18] N. Majlis, S. Selzer, and G. C. Strinati, Phys. Rev. B **45**, 7872 (1992); **48**, 957 (1993); H. Rosner, H. Eschrig, R. Hayn, S.-L. Drechsler, and J. Malek, *ibid.* **56**, 3402 (1997).

[19] H. J. Schulz, Phys. Rev. Lett. **77**, 2790 (1996); Z. Wang, *ibid.* **78**, 126 (1997).

[20] A. W. Sandvik, Phys. Rev. Lett. **83**, 3069 (1999).

[21] Y. J. Kim and R. J. Birgeneau, Phys. Rev. B **62**, 6378 (2000).

[22] W. Li, S.-S. Gong, Y. Zhao, and G. Su, Phys. Rev. B **81**, 184427 (2010).

[23] F. Jiang and U. Gerber, J. Stat. Mech. (2009) P09016.

[24] Y.-Z. Huang, B. Xi, X. Chen, W. Li, Z.-C. Wang, and G. Su, Phys. Rev. E **93**, 062110 (2016).

[25] Y. Zhao, W. Li, B. Xin, S.-J. Ran, Y.-Y. Zhu, B.-W. Wang, S. Gao, and G. Su, Europhys. Lett. **104**, 57009 (2013).

[26] N. V. Prokof'ef, B. V. Svistunov, and I. S. Tupitsyn, Sov. Phys.-JETP **87**, 310 (1998).

[27] B. Xi, S. Hu, J. Zhao, G. Su, B. Normand, and X. Wang, Phys. Rev. B **84**, 134407 (2011).

[28] A. W. Sandvik, AIP Conf. Proc. **1297**, 135 (2010).

[29] M. E. Fisher, M. N. Barber, and D. Jasnow, Phys. Rev. A **8**, 1111 (1973).

[30] B. D. Josephson, Phys. Lett. **21**, 608 (1966).

[31] S. Todo and K. Kato, Phys. Rev. Lett. **87**, 047203 (2001).

[32] S. Yasuda, H. Suwa, and S. Todo, Phys. Rev. B **92**, 104411 (2015).

[33] M. Campostrini, M. Hasenbusch, A. Pelissetto, P. Rossi, and E. Vicari, Phys. Rev. B **65**, 144520 (2002).

[34] K. Binder, Phys. Rev. Lett. **47**, 693 (1981).

[35] K. Binder, Z. Phys. B: Condens. Matter **43**, 119 (1981).

[36] K. Binder and D. P. Landau, Phys. Rev. B **30**, 1477 (1984).

[37] N. Schultka and E. Manousakis, Phys. Rev. B **49**, 12071 (1994).

[38] N. Schultka and E. Manousakis, Phys. Rev. B **51**, 11712 (1995).

[39] L. Wang, K. S. D. Beach, and A. W. Sandvik, Phys. Rev. B **73**, 014431 (2006).

[40] E. Brézin, J. Physique **43**, 15 (1982).

[41] M. N. Barber, in *Phase Transitions and Critical Phenomena*, edited by C. Domb and J. L. Lebowitz (Academic Press, New York, 1983), Vol. 8.

[42] E. Brézin and J. Zinn-Justin, Nucl. Phys. B **257**, 867 (1985).

[43] K. S. D. Beach, L. Wang, and A. W. Sandvik, arXiv:cond-mat/0505194.

[44] P. R. Gill, W. Murray, and M. H. Wright, *Practical Optimization* (Academic Press, San Diego, 1988).

[45] M. E. Fisher and M. N. Barber, Phys. Rev. Lett. **28**, 1516 (1972)

[46] M. Campostrini, M. Hasenbusch, A. Pelissetto, P. Rossi, and E. Vicari, Phys. Rev. B **63**, 214503 (2001)

[47] https://lmfit.github.io/lmfit-py.

[48] A. Klümper, Eur. Phys. J. B **5**, 677 (1998).

[49] B. Gu, G. Su, and S. Gao, Phys. Rev. B **73**, 134427 (2006); S. S. Gong, S. Gao, and G. Su, *ibid.* **80**, 014413 (2009).

[50] J. M. Kosterlitz and D. J. Thouless, J. Phys. C **5**, L124 (1972).

[51] Y.-Da Hsieh, Y.-Jer Kao, A. W. Sandvik, J. Stat. Mech. (2013) P09001.